Time-Reversal Division Multiple Access over Multi-Path Channels

Feng Han, *Student Member, IEEE,* Yu-Han Yang, *Student Member, IEEE,* Beibei Wang, *Member, IEEE,* Yongle Wu, *Member, IEEE,* and K. J. Ray Liu, *Fellow, IEEE*

***Abstract*—The multi-path effect makes high speed broadband communications a very challenging task due to the severe inter-symbol interference (ISI). By concentrating energy in both the spatial and temporal domains, time-reversal (TR) transmission technique provides a great potential of low-complexity energy-efficient communications. In this paper, a novel concept of time-reversal division multiple access (TRDMA) is proposed as a wireless channel access method based on its high-resolution spatial focusing effect. It is proposed to use TR structure in multi-user downlink systems over multi-path channels, where signals of different users are separated solely by TRDMA. Both the single-transmit-antenna scheme and its enhanced version with multiple transmit antennas are developed and evaluated in this paper. The system performance is investigated in terms of its effective signal-to-interference-plus-noise ratio (SINR), the achievable sum rate and the achievable rates with outage. And some further discussions regarding its advantage over conventional rake receivers and the impact of spatial correlations between users are given at the end of this paper. It is shown in both analytical and simulation results that desirable properties and satisfying performances can be achieved in the proposed TRDMA multi-user downlink system, which makes TRDMA a promising candidate for future energy-efficient low-complexity broadband wireless communications.**

***Index Terms*—Time Reversal, temporal focusing, spatial focusing, TRDMA.**

I. Introduction

THE past decade has witnessed an unprecedent increase of demand for high speed wireless services, which necessitates the need for future broadband communications. When it comes to broadband, the resolution of perceiving multiple paths increases accordingly. In a rich scattering environment, the adverse multi-path effect makes conventional high-speed communications a very challenging task due to the severe inter-symbol interference (ISI). To resolve this problem, multi-carrier modulation (e.g. OFDM) and/or complicated equalization are needed [1]–[4] at the receiver to alleviate the ISI. Although the performance is well satisfactory, it often results in a prohibitively high complexity for end-user equipments and wireless terminals in many applications.

Paper approved by D. I. Kim, the Editor for Spread Spectrum Transmission and Access of the IEEE Communications Society. Manuscript received August 12, 2011; revised January 4, 2012.

F. Han, Y.-H. Yang, and K. J. R. Liu are with the Department of Electrical and Computer Engineering, University of Maryland, College Park, MD, 20742 USA (e-mail: {hanf, yhyang, kjrliu}@umd.edu).

B. Wang and Y. Wu are with Qualcomm Inc., San Diego, CA, 92121, USA (e-mail: {beibeiw, yonglew}@qualcomm.com).

Digital Object Identifier 10.1109/TCOMM.2012.051012.110531

On the other hand, time-reversal (TR) signal transmission technique can provide a great potential of low-complexity energy-efficient communications[5], which can make full use of the nature of multi-path environments. The history of research on time-reversal transmission technology dates back to early 1990's[6]–[10]; however, not much development and interest went beyond the acoustics and ultrasound domains at that time. As found in acoustic physics [6]–[10] and then further validated in practical underwater propagation environments[11]–[13], the energy of the TR acoustic waves from transmitters could be refocused only at the intended location with very high spatial resolution (several-wavelength level). Since TR can make full use of multi-path propagation and also requires no complicated channel processing and equalization, it was later verified and tested in wireless radio communication systems, especially in Ultra-wideband (UWB) systems[14]–[18].

The single-user TR wireless communications consist of two phases: the *recording phase* and the *transmission phase*. When transceiver A wants to transmit information to transceiver B, transceiver B first sends an impulse that propagates through a scattering multi-path environment and the multi-path signals are received and recorded by transceiver A; then, transceiver A simply transmits the time-reversed (and conjugated) waves back through the communication link to transceiver B. By utilizing channel reciprocity[19], the TR waves can retrace the incoming paths, ending up with a "spiky" signal-power spatial distribution focused only at the intended location, as commonly referred to as *spatial focusing effect*[5][17]. Also, from a signal processing point of view, in single-user communications, TR essentially leverages the multi-path channel as a facilitating matched filter computing machine for the intended receiver, and concentrates the signal energy in the time domain as well, as commonly referred to as *temporal focusing effect*. It is worth noting that when the channel coherent time is not very small, the transmission phase of a duty cycle can include multiple transmissions of signals without requiring probing the channel before each transmission, which can reasonably maintain the bandwidth efficiency. It is typically the case when TR is used, and was verified by real-life experiments in [5].

In the single-user case, the temporal and spatial focusing effects have been shown to greatly simplify the receiver[14]–[18], [23], [24], and reduce power consumption and interference while maintaining the quality of service (QoS)[5]. In this paper, we consider a multi-user downlink system over multi-path channels, and propose a concept of time-reversal

division multiple access (TRDMA) as a wireless channel access method by taking advantage of the high-resolution spatial focusing effect of time-reversal structure. In principle, the mechanisms of reflection, diffraction and scattering in wireless medium give rise to the uniqueness and independence of the multi-path propagation profile of each communication link[19], which are exploited to provide spatial selectivity in spatial division multiple access (SDMA) schemes. Compared with conventional antenna-array based beamforming SDMA schemes, time-reversal technique makes full use of a large number of multi-paths and in essence treats each path as a virtual antenna that naturally exists and is widely distributed in environments.

Thus, with even just one single transmit antenna, time reversal can potentially achieve a very high diversity gain and high-resolution "pin-point" spatial focusing. The high-resolution spatial focusing effect maps the natural multi-path propagation profile into a unique *location-specific signature* for each link, as an analogy to the artificial "orthogonal random code" in a code-division system. The proposed TRDMA scheme exploits the uniqueness and independence of location-specific signatures in multi-path environment, providing a novel low-cost energy-efficient solution for SDMA. Better yet, the TRDMA scheme accomplishes much higher spatial-resolution focusing/selectivity and time-domain signal-energy compression at once, without requiring further equalization at the receiver as the antenna-array based beamforming does.

The potential and feasibility of applying time reversal to multi-user UWB communications were validated by some real-life antenna-and-propagation experiments in[5], [20]–[22], in which the signal transmit power reduction and inter-user interference alleviation as a result of spatial focusing effect were tested and justified for one simplified *one-shot* transmission over deterministic multi-path ultra-wideband channels. The idea of TRDMA proposed in this paper was further supported by several important recent works [23]–[25]. [23] introduced a TR-based single-user spatial multiplexing scheme for SIMO UWB system, in which multiple data streams are transmitted through one transmit antenna and received by a multi-antenna receiver. Solid simulation results regarding bit-error-ratio (BER) demonstrate the feasibility of applying TR to spatially multiplex data streams. Following [23], [24] took into account the spatial correlation between antennas of the single receiver and numerically investigated through computer simulation its impact to BER performance. Based on [23] and [24], [25] tackled a multiuser UWB scenario with a focus on the impact of channel correlation to the BER performance through simulation. However, there is not much theoretical characterization or proof about system performances found in any of these papers. Furthermore, most of these literatures focus only on BER performances, without looking at the spectral efficiency which is one of the main design purposes for any spatial multiplexing scheme. There is still a lack of system-level theoretical investigation and comprehensive performance analysis of a TR-based multi-user communications system in the literature. Motivated by the high-resolution spatial focusing potential of the time-reversal structure, existing experimental measurements and supporting literatures, several major developments have been proposed and considered in the proposed TRDMA multi-user communications system. Specifically:

- We propose the concept of TRDMA as a novel multi-user downlink solution for wireless multi-path environments, and developed a theoretical analysis framework for the proposed scheme.
- We consider a multi-user broadband communication system over multi-path *Rayleigh fading* channels, in which the signals of multiple users are separated solely by TRDMA.
- We define and evaluate a number of system performance metrics, including the effective SINR at each user, achievable sum rate, and achievable rate with $\epsilon-$outage.
- We further investigate the achievable rate region for a simplified two-user case, from which one can see the advantages of TRDMA over its counterpart techniques, due to TR's spatial focusing effect.
- We incorporate and examine quantitatively the impact of spatial correlation of users to system performances for the SISO case to gain more comprehensive understanding of TRDMA.

The rest of this paper is organized as follows. In Section II, we introduce the channel model and the proposed TRDMA multi-user downlink systems with both a single transmit antenna and multiple antennas. Then, we analyze the effective SINR in Section III. In Section IV, both achievable sum rate and $\epsilon-$outage rate are evaluated. Also in Section IV, a two-user case achievable rate region is characterized and compared with the rake-receiver counterparts. In Section V, the impact of spatial correlation between users is investigated and discussed. Finally, conclusions are drawn in Section VI.

II. System Model

In this section, we introduce the channel and system model and the proposed TRDMA schemes. We begin with the assumptions and formulations of the channel model. Then, we describe the two phases of the basic TRDMA scheme with a single transmit antenna. Finally, we extend the basic single-input-single-output (SISO) scheme to an enhanced multiple-input-single-output (MISO) TRDMA scheme with multiple transmit antennas at the base station (BS).

A. Channel Model

In this paper, we consider a multi-user downlink network over multi-path Rayleigh fading channels. We first look at a SISO case where the base station (BS) and all users are equipped with a single antenna. The channel impulse response (CIR) of the communication link between the BS and the i-th user is modeled as

$$h_i[k] = \sum_{l=0}^{L-1} h_{i,l}\delta[k-l], \tag{1}$$

where $h_i[k]$ is the k-th tap of the CIR with length L, and $\delta[\cdot]$ is the Dirac delta function. For each link, we assume that $h_i[k]$'s are independent circular symmetric complex Gaussian (CSCG) random variables with zero mean and variance

$$E[|h_i[k]|^2] = e^{-\frac{kT_S}{\sigma_T}}, \quad 0 \leqslant k \leqslant L-1 \tag{2}$$

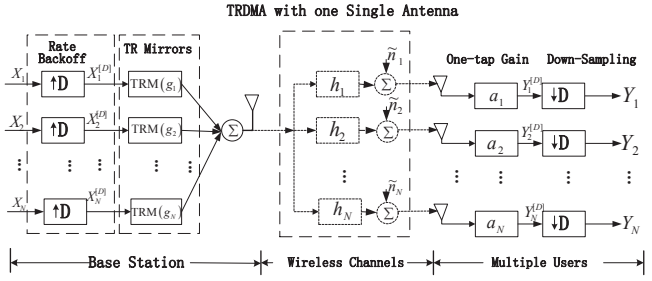

Fig. 1. The diagram of SISO TRDMA multiuser downlink system.

where T_S is the sampling period of this system such that $1/T_S$ equals the system bandwidth B, and σ_T is the root mean square (rms) delay spread[3] of the channel. Due to the two-phase nature of TR structure, we assume that channels are reciprocal, ergodic and blockwise-constant with their tap values remaining fixed during at least one duty cycle. Each duty cycle consists of the recording phase and the transmission phase, which occupy the proportions of $(1-\eta)$ and η of the cycle period, with $\eta \in (0,1)$ depending on how fast channels vary over time.

We first assume that the CIRs associated with different users are uncorrelated. While realistic CIRs might not be perfectly uncorrelated, this assumption greatly simplifies the analysis while capturing the essential idea of TRDMA. Moreover, real-life experimental results in [5], [17] show that in a rich-scattering environment the correlation between CIRs associated with different locations decreases to a neglectable level when two locations are even just several wave-lengths apart. A further discussion on the impact of the channel correlation between users to the system performance will be addressed in Section V.

B. Phase 1: Recording Phase

The block diagram of a SISO TRDMA downlink system is shown in Fig. 1, in which there are N users receiving statistically independent messages $\{X_1(k), X_2(k), \cdots, X_N(k)\}$ from the BS, respectively. The time-reversal mirror (TRM) shown in the diagram is a device that can record and time-reverse (and conjugate if complex-valued) the received waveform, which will be used to modulate the time-reversed waveform with input signal by convolving them together in the following transmission phase.

During the recoding phase, the N intended users first take turns to transmit an impulse signal to the BS (ideally it can be a Dirac $\delta-$function, but in practice a modified raise-cosine signal can be a good candidate for limited bandwidth for this purpose[5]). Meanwhile, the TRMs at the BS record the channel response of each link and store the time-reversed and conjugated version of each channel response for the transmission phase. For simplicity of analytical derivation, we assume in our analysis that the waveform recorded by TRM reflects the true CIR, ignoring the small corruption caused by thermal noise and quantization noise. Such a simplification was justified and based on the following facts shown in literatures of time reversal:

- The thermal noise (typically modeled as additive white Gaussian noise (AWGN)) can be effectively reduced to a desired level by averaging multiple recorded noisy samples of the same CIR's, provided that channels are slow-varying, as shown in the real-life experiments [5]. This would increase the portion $(1-\eta)$ of the recording phase in the entire duty cycle, leading to a increased channel probing overhead; but the structure of the analysis for the proposed system is not altered.
- The effect of quantization was studied by [26]. It was shown that a nine-bit quantization can be treated as nearly perfect for most applications; and even with one-bit quantization, the TR system can work reasonably well, demonstrating the robustness of the TR-based transmission technique.

C. Phase 2: Transmission Phase

After the channel recording phase, the system starts its transmission phase. At the BS, each of $\{X_1, X_2, \cdots, X_N\}$ represents a sequence of information symbols that are independent complex random variables with zero mean and variance of θ. In other words, we assume that for each i from 1 to N, $X_i[k]$ and $X_i[l]$ are independent when $k \neq l$. As we mentioned earlier, any two sequences of $\{X_1, X_2, \cdots, X_N\}$ are also independent in our model. We introduce the rate back-off factor D as the ratio of the sampling rate to the baud rate, by performing up-sampling and down-sampling with a factor D at the BS and receivers as shown in Fig. 1. Such a notion of back-off factor facilitates simple rate conversion in the analysis of a TR system.

These sequences are first up-sampled by a factor of D at the BS, and the i-th up-sampled sequence can be expressed as

$$X_i^{[D]}[k] = \begin{cases} X_i[k/D], & \text{if } k \bmod D = 0, \\ 0, & \text{if } k \bmod D \neq 0. \end{cases} \tag{3}$$

Then the up-sampled sequences are fed into the bank of TRMs $\{g_1, g_2, \cdots, g_N\}$, where the output of the i-th TRM g_i is the convolution of the i-th up-sampled sequence $\left\{X_i^{[D]}[k]\right\}$ and the TR waveform $\{g_i[k]\}$ as shown in Fig. 1, with

$$g_i[k] = h_i^*[L-1-k] \Bigg/ \sqrt{E\left[\sum_{l=0}^{L-1} |h_i[l]|^2\right]}, \tag{4}$$

which is the normalized (by the average channel gain) complex conjugate of time-reversed $\{h_i[k]\}$. After that, all the outputs of TRM bank are added together, and then the combined signal $\{S[k]\}$ is transmitted into wireless channels with

$$S[k] = \sum_{i=1}^{N} \left(X_i^{[D]} * g_i\right)[k]. \tag{5}$$

In essence, by convolving the information symbol sequences with TR waveforms, TRM provides a mechanism of embedding the unique location-specific signature associated with each communication link into the transmitted signal for the intended user.

The signal received at user i is represented as follows

$$Y_i^{[D]}[k] = \sum_{j=1}^{N} \left(X_j^{[D]} * g_j * h_i\right)[k] + \tilde{n}_i[k], \tag{6}$$

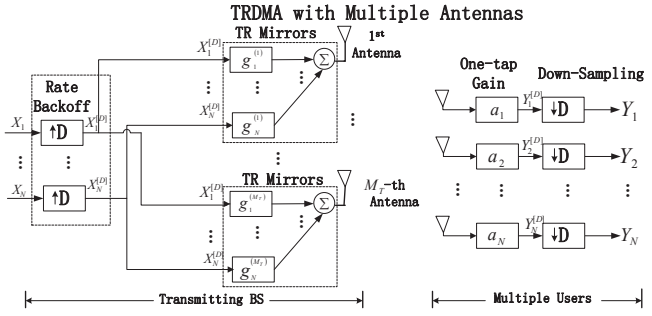

Fig. 2. The diagram of MISO TRDMA multiuser downlink system.

which is the convolution of the transmitted signal $\{S[k]\}$ and the CIR $\{h_i[k]\}$, plus an additive white Gaussian noise sequence $\{\tilde{n}_i[k]\}$ with zero mean and variance σ^2.

Thanks to the temporal focusing effect, the signal energy is concentrated in a single time sample. The i-th receiver (user i) simply performs a one-tap gain adjustment a_i to the received signal to recover the signal and then down-samples it with the same factor D, ending up with $Y_i[k]$ given as follows (for notational simplicity, $L-1$ is assumed to be a multiple of D)

$$Y_i[k] = a_i \sum_{j=1}^{N} \sum_{l=0}^{(2L-2)/D} (h_i * g_j)[Dl] X_j[k-l] + a_i n_i[k], \quad (7)$$

where

$$(h_i * g_j)[k] = \sum_{l=0}^{L-1} h_i[l] g_j[k-l] = \frac{\sum_{l=0}^{L-1} h_i[l] h_j^*[L-1-k+l]}{\sqrt{E\left[\sum_{l=0}^{L-1} |h_j[l]|^2\right]}} \quad (8)$$

with $k = 0, 1, \cdots, 2L-2$, and $n_i[k] = \tilde{n}_i[Dk]$, which is AWGN with zero mean and variance σ^2.

D. TRDMA with multiple transmit antennas

In this part, we generalize the basic TRDMA scheme into an enhanced version with multiple transmit antennas. To maintain low complexity at receivers, we consider a MISO case where the transmitting BS is equipped with M_T antennas together with multiple single-antenna users.

Let $h_i^{(m)}[k]$ denote the k-th tap of the CIR for the communication link between user i and the m-th antenna of the BS, and we assume it is a circular symmetric complex Gaussian random variable with zero mean and a variance

$$E[|h_i^{(m)}[k]|^2] = e^{-\frac{kT_S}{\sigma_T}}. \quad (9)$$

In alignment with the basic SISO case, we also assume that paths associated with different antennas are uncorrelated, i.e. $h_i^{(m)}[k]$ and $h_j^{(w)}[l]$ are uncorrelated for $\forall\, i, j \in \{1, 2, \cdots, N\}$ and $\forall\, k, l \in \{0, 1, \cdots, L-1\}$ when $m \neq w$, where $m, w \in \{1, 2, \cdots, M_T\}$ are the indices of the m-th and w-th antennas at the BS.

For the MISO TRDMA scheme, each antenna at the BS plays a role similar to the single-antenna BS in the basic scheme. The block diagram for the MISO TRDMA is shown in Fig. 2. The TR waveform $\{g_i^{(m)}[k]\}$ is the normalized (by the average total energy of MISO channels) complex conjugate of time-reversed $\{h_i^{(m)}[k]\}$, i.e.

$$g_i^{(m)}[k] = h_i^{(m)*}[L-1-k] \Big/ \sqrt{E\left[M_T \sum_{l=0}^{L-1} |h_i^{(m)}[l]|^2\right]}. \quad (10)$$

As a result, the average total transmit power at the BS is

$$P = \frac{N \times \theta}{D}, \quad (11)$$

which does not depend on the number of the transmit antennas M_T.

The resulting received signal at user i can be similarly represented as

$$Y_i[k] = \sum_{j=1}^{N} \sum_{m=1}^{M_T} \sum_{l=0}^{\frac{2L-2}{D}} \left(h_i^{(m)} * g_j^{(m)}\right)[Dl] X_j[k-l] + n[k], \quad (12)$$

where $n[k]$ is additive white Gaussian noise with zero mean and variance σ^2.

Hereafter, we define a modified received signal-to-noise ratio (SNR) ρ for the

$$\rho = \frac{P}{\sigma^2} E\left[\sum_{l=0}^{L-1} |h_i^{(m)}[l]|^2\right] = \frac{P}{\sigma^2} \frac{1 - e^{-\frac{LT_S}{\sigma_T}}}{1 - e^{-\frac{T_S}{\sigma_T}}}, \quad (13)$$

to rule out the potential multi-path gain in the system model in the following performance evaluations.

In the following sections, we evaluate the system performance of the proposed system in terms of the effective SINR, the achievable sum rate, and the achievable rates with $\epsilon-$outage.

III. Effective SINR

In this section, we evaluate the effective SINR of the proposed system. Since the basic SISO scheme is just a special case with $M_T = 1$, we analyze the general MISO case with M_T as a parameter in this section.

Note that for $\left\{(h_i^{(m)} * g_j^{(m)})[k]\right\}$ in (12), when $k = L-1$ and $j = i$, it corresponds to the maximum-power central peak of the autocorrelation function, i.e.

$$(h_i^{(m)} * g_i^{(m)})[L-1] = \sum_{l=0}^{L-1} |h_i^{(m)}[l]|^2 \Big/ \sqrt{E\left[M_T \sum_{l=0}^{L-1} |h_i^{(m)}[l]|^2\right]}. \quad (14)$$

Subject to the constraint of one-tap receivers, the i-th receiver is designed to estimate $X_i[k - \frac{L-1}{D}]$ solely based on the observation of $Y_i[k]$. Then, the remaining components of Y_i can be further categorized into inter-symbol interference (ISI), inter-user interference (IUI) and noise, as shown below:

$$\begin{aligned} Y_i[k] = {} & a_i \sum_{m=1}^{M_T} (h_i^{(m)} * g_i^{(m)})[L-1] X_i[k - \frac{L-1}{D}] \quad (Signal) \\ & + a_i \sum_{\substack{l=0 \\ l \neq (L-1)/D}}^{(2L-2)/D} \sum_{m=1}^{M_T} (h_i^{(m)} * g_i^{(m)})[Dl] X_i[k-l] \quad (ISI) \\ & + a_i \sum_{\substack{j=1 \\ j \neq i}}^{N} \sum_{l=0}^{(2L-2)/D} \sum_{m=1}^{M_T} (h_i^{(m)} * g_j^{(m)})[Dl] X_j[k-l] \quad (IUI) \\ & + a_i n_i[k]. \quad (Noise) \end{aligned} \quad (15)$$

Note that the one-tap gain a_i does not affect the effective SINR, we consider it as $a_i = 1$ in the subsequent analysis, without loss of generality.

Given a specific realization of the random CIRs, from (15), one can calculate the signal power $P_{Sig}(i)$ as

$$P_{Sig}(i) = E_X\left[\left|\sum_{m=1}^{M_T}(h_i * g_i)[L-1]X_i[k-\frac{L-1}{D}]\right|^2\right] \quad (16)$$
$$= \theta\left|\sum_{m=1}^{M_T}\left(h_i^{(m)} * g_i^{(m)}\right)[L-1]\right|^2,$$

where $E_X[\cdot]$ represents the expectation over X. Accordingly, the powers associated with ISI and IUI can be derived as

$$P_{ISI}(i) = \theta\sum_{\substack{l=0 \\ l\neq\frac{L-1}{D}}}^{\frac{2L-2}{D}}\left|\sum_{m=1}^{M_T}\left(h_i^{(m)} * g_i^{(m)}\right)[Dl]\right|^2, \quad (17)$$

$$P_{IUI}(i) = \theta\sum_{\substack{j=1 \\ j\neq i}}^{N}\sum_{l=0}^{\frac{2L-2}{D}}\left|\sum_{m=1}^{M_T}\left(h_i^{(m)} * g_j^{(m)}\right)[Dl]\right|^2. \quad (18)$$

When there exists interference, the SINR is almost always a crucial performance metric used to measure the extent to which a signal is corrupted. It is especially the case for a media-access scheme, where interference management is one of the main design objectives. In this part, we investigate the *effective SINR* at each user in this multi-user network.

We define the average *effective SINR* at user i $SINR_{avg}(i)$ as the ratio of the average signal power to the average interference-and-noise power, i.e.,

$$SINR_{avg}(i) = \frac{E\left[P_{Sig}(i)\right]}{E\left[P_{ISI}(i)\right] + E\left[P_{IUI}(i)\right] + \sigma^2}, \quad (19)$$

where each term has been specified in (16), (17) and (18). Note that such defined *effective SINR* in (19) bears difference with the quantity $E\left[\frac{P_{Sig}(i)}{P_{ISI}(i)+P_{IUI}(i)+\sigma^2}\right]$ in general. The former can be treated as an approximation of the latter quantity. Such an approximation is especially useful when the calculation of the average SINR using multiple integration is too complex, as is the case in this paper and literatures such as [18], [28], [29]. The performance of this approximation will be demonstrated in the numerical results shown in Figures 3, 4 and 5.

Theorem 1. *For the independent multi-path Rayleigh fading channels given in Section II, the expected value of each term for the average effective SINR (19) at user i can be obtained as shown in (20), (21), and (22).*

Proof: Based on the channel model presented in Section II, the second and fourth moments of $h_i^{(m)}[k]$ are given by[36]

$$E\left[|h_i^{(m)}[k]|^2\right] = e^{-\frac{kT_S}{\sigma_T}}, \quad (23)$$

$$E\left[|h_i^{(m)}[k]|^4\right] = 2\left(E\left[|h_i^{(m)}[k]|^2\right]\right)^2 = 2e^{-\frac{2kT_S}{\sigma_T}}. \quad (24)$$

Based on (23) and (24), after some basic mathematical derivations, we obtain the following expected values for $\forall i \in \{1, 2, \cdots, N\}$ in (25), (26), and (27).

Therefore, according to (16-18), (20-22) are obtained as shown in Theorem 1. ∎

From Theorem 1, one can see that the average interference powers (i.e. ISI and IUI) in (26) and (27) do not depend on M_T, while the signal power level in (25) increases linearly with the number of antennas, which is due to an enhanced focusing capability with multiple transmit antennas leveraging the multi-paths in the environment. The enhanced focusing effects monotonically improve the effective SINR. Another interesting observation is that a larger back-off factor D yields higher reception quality of each symbol, which is especially effective in the high SINR regime where interference power dominates the noise power. The asymptotic behavior of the SINR in the high SNR regime with varying D is given by the following theorem.

Theorem 2. *In the high SNR regime, when D is small such that $D \ll L$ and $D \ll \sigma_T/T_S$, doubling D leads to approximately a 3dB gain in the average effective SINR.*

Proof: First note that the signal power does not depend on D and that the noise is negligible in the high SINR regime. Thus, we can focus on the interference powers.

- **For Inter-Symbol Interference (ISI)**:

$$\frac{E\left[P_{ISI}(i, D=d)\right]}{E\left[P_{ISI}(i, D=2d)\right]} = \left(1+e^{-\frac{dT_S}{\sigma_T}}\right)\frac{\left(1-e^{-\frac{(L-2+d)T_S}{\sigma_T}}\right)}{\left(1-e^{-\frac{(L-2+2d)T_S}{\sigma_T}}\right)} \quad (28)$$

Since $D \ll L$, then $\frac{\left(1-e^{-\frac{(L-2+d)T_S}{\sigma_T}}\right)}{\left(1-e^{-\frac{(L-2+2d)T_S}{\sigma_T}}\right)} \approx 1$; and since $D \ll \frac{\sigma_T}{T_S}$, then $e^{-\frac{dT_S}{\sigma_T}} \approx 1$. Therefore,

$$\frac{E\left[P_{ISI}(i, D=d)\right]}{E\left[P_{ISI}(i, D=2d)\right]} \approx 2.$$

- **For Inter-User Interference (IUI)**:

$$\frac{E\left[P_{IUI}(i, D=d)\right]}{E\left[P_{IUI}(i, D=2d)\right]} = \left(1+e^{-\frac{dT_S}{\sigma_T}}\right) \times \quad (29)$$
$$\frac{\left(1+e^{-\frac{dT_S}{\sigma_T}}\right)\left(1+e^{-\frac{2LT_S}{\sigma_T}}\right) - 2e^{-\frac{(L+1)T_S}{\sigma_T}}\left(1+e^{-\frac{(d-2)T_S}{\sigma_T}}\right)}{\left(1+e^{-\frac{2dT_S}{\sigma_T}}\right)\left(1+e^{-\frac{2LT_S}{\sigma_T}}\right) - 2e^{-\frac{(L+1)T_S}{\sigma_T}}\left(1+e^{-\frac{(2d-2)T_S}{\sigma_T}}\right)}.$$

For similar reasons,

$$\frac{E\left[P_{IUI}(i, D=d)\right]}{E\left[P_{IUI}(i, D=2d)\right]} \approx 2.$$

∎

Next, we present some numerical evaluation of the average effective SINR. In this paper, we mainly consider the broadband systems with frequency bandwidth that typically ranges from hundreds MHz to several GHz, which is much wider that those narrow-band systems specified in 3GPP/3GPP2. In the rich scattering environment, the underlying paths are so many that the number of perceived multiple paths increases quickly with the system bandwidth. For a system with bandwidth B, the minimum resolvable time-difference between two paths is $T_S = 1/B$[4]. Keeping this in mind, we first choose $L = 257$ and $\sigma_T = 128T_S$ from a typical range, and

$$E\left[P_{Sig}(i)\right] = \theta\frac{1+e^{-\frac{LT_S}{\sigma_T}}}{1+e^{-\frac{T_S}{\sigma_T}}} + \theta M_T\frac{1-e^{-\frac{LT_S}{\sigma_T}}}{1-e^{-\frac{T_S}{\sigma_T}}}; \tag{20}$$

$$E\left[P_{ISI}(i)\right] = 2\theta\frac{e^{-\frac{T_S}{\sigma_T}}\left(1-e^{-\frac{(L-2+D)T_S}{\sigma_T}}\right)}{\left(1-e^{-\frac{DT_S}{\sigma_T}}\right)\left(1+e^{-\frac{T_S}{\sigma_T}}\right)}; \tag{21}$$

$$E\left[P_{IUI}(i)\right] = \theta(N-1)\frac{\left(1+e^{-\frac{DT_S}{\sigma_T}}\right)\left(1+e^{-\frac{2LT_S}{\sigma_T}}\right) - 2e^{-\frac{(L+1)T_S}{\sigma_T}}\left(1+e^{-\frac{(D-2)T_S}{\sigma_T}}\right)}{\left(1-e^{-\frac{DT_S}{\sigma_T}}\right)\left(1+e^{-\frac{T_S}{\sigma_T}}\right)\left(1-e^{-\frac{LT_S}{\sigma_T}}\right)}. \tag{22}$$

$$E\left[\left|\sum_{m=1}^{M_T}\left(h_i^{(m)} * g_i^{(m)}\right)[L-1]\right|^2\right] = \frac{1+e^{-\frac{LT_S}{\sigma_T}}}{1+e^{-\frac{T_S}{\sigma_T}}} + M_T\frac{1-e^{-\frac{LT_S}{\sigma_T}}}{1-e^{-\frac{T_S}{\sigma_T}}}; \tag{25}$$

$$E\left[\sum_{\substack{l=0\\ l\neq\frac{L-1}{D}}}^{\frac{2L-2}{D}}\left|\sum_{m=1}^{M_T}\left(h_i^{(m)} * g_i^{(m)}\right)[Dl]\right|^2\right] = 2\frac{e^{-\frac{T_S}{\sigma_T}}\left(1-e^{-\frac{(L-2+D)T_S}{\sigma_T}}\right)}{\left(1-e^{-\frac{DT_S}{\sigma_T}}\right)\left(1+e^{-\frac{T_S}{\sigma_T}}\right)}, \tag{26}$$

$$E\left[\sum_{\substack{j=1\\ j\neq i}}^{N}\sum_{l=0}^{\frac{2L-2}{D}}\left|\sum_{m=1}^{M_T}\left(h_j^{(m)} * g_i^{(m)}\right)[Dl]\right|^2\right] = (N-1)\frac{\left(1+e^{-\frac{DT_S}{\sigma_T}}\right)\left(1+e^{-\frac{2LT_S}{\sigma_T}}\right) - 2e^{-\frac{(L+1)T_S}{\sigma_T}}\left(1+e^{-\frac{(D-2)T_S}{\sigma_T}}\right)}{\left(1-e^{-\frac{DT_S}{\sigma_T}}\right)\left(1+e^{-\frac{T_S}{\sigma_T}}\right)\left(1-e^{-\frac{LT_S}{\sigma_T}}\right)}. \tag{27}$$

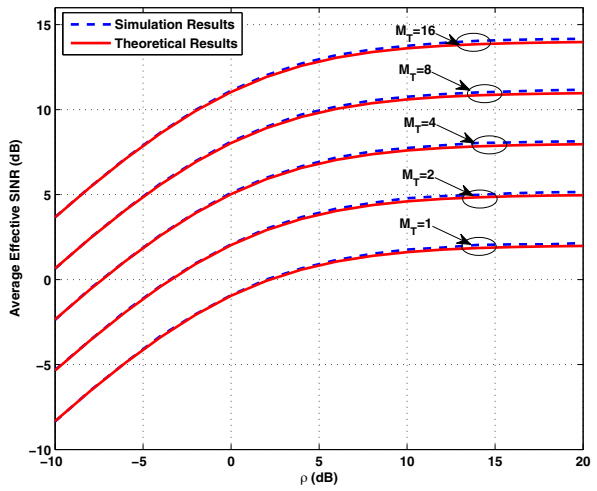

Fig. 3. The impact of the number of antennas when $D = 8,\ N = 5$.

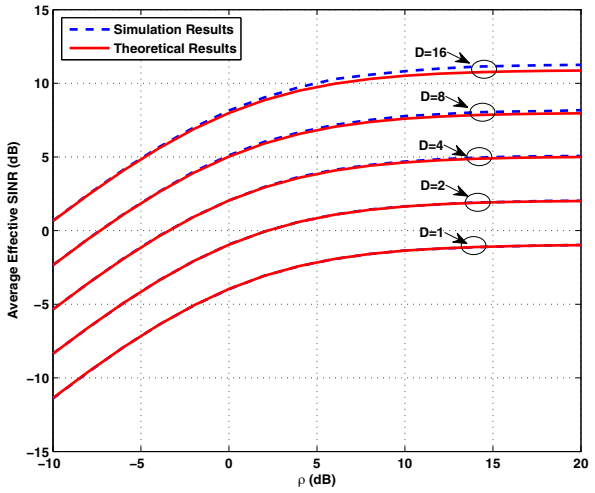

Fig. 4. The impact of the rate back-off factor when $N = 5,\ M_T = 4$.

evaluate the average effective SINR versus ρ under various system configurations in terms of N (the number of users), M_T (the number of antennas) and D (the rate back-off factor). In Fig. 3, Fig. 4 and Fig. 5, with $L = 257$ and $\sigma_T = 128T_S$, the solid curves are obtained according to the analytical results given by Theorem 1, and the dashed curves are collected from simulation which numerically computes $E\left[\frac{P_{Sig}(i)}{P_{ISI}(i)+P_{IUI}(i)+\sigma^2}\right]$. One can see that the results shown in Theorem 1 approximate well the empirical means obtained by simulation, which demonstrates the effectiveness of the definition of effective SINR in the system of interest in this paper.

Fig. 3 is plotted with $D = 8$ and $N = 5$, demonstrating the impact of the number of antennas M_T to the effective SINR. From Fig. 3, one can see that approximately a 3dB gain is attained as M_T is doubled within a reasonable range. The impact of the rate back-off to the effective SINR is shown with $N = 5,\ M_T = 4$ in Fig. 4. Both analytical formulas and simulation results show that a lager D can reduce ISI and IUI while maintaining the signal power. In the high SNR regime where interference powers dominates the noise power,

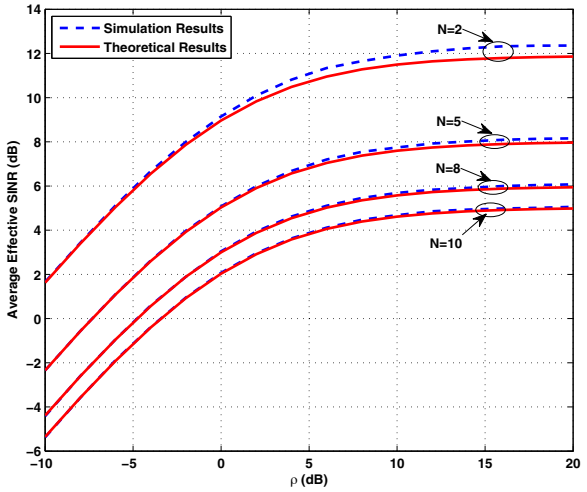

Fig. 5. The impact of the number of users when $D = 8,\ M_T = 4$.

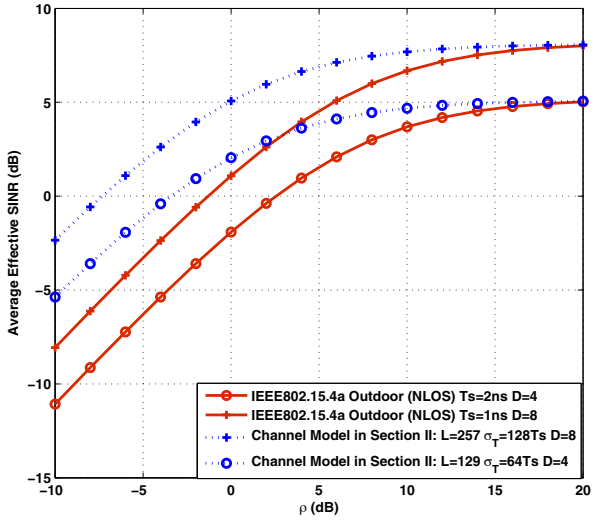

Fig. 6. Average Effective SINR for IEEE 802.15.4a outdoor NLOS channel models.

approximately a 3dB gain in effective SINR can be seen when D is doubled in Fig. 4, as predicted in Theorem 2. In Fig. 5, we investigate the impact of the number of users with $D = 8,\ M_T = 4$. Due to the existence of IUI, increasing the number of co-existing users will result in higher interference between users. That implies a tradeoff between the network capacity (in terms of number of serviced users) and signal reception quality at each user, as indicated in Fig. 5.

Furthermore, to demonstrate the usefulness and practical importance of TRDMA, we apply the proposed scheme to more practical channel models, the IEEE 802.15.4a outdoor non-line-of-sight (NLOS) channels, operating over bandwidth of $B = 500$ MHz ($T_S = 2$ ns and the typical channel length $L \sim 80$ to 150 taps) and $B = 1$ GHz ($T_S = 1$ ns and the typical channel length $L \sim 200$ to 300 taps) , respectively. Fig. 6 shows the performances of the proposed TRDMA scheme over the two aforementioned more practical channel models with $M_T = 4$. Such two practical channel models have comparable system bandwidth and channel lengths with the systems which TRDMA is designed for. From Fig. 6, one can see that the performances for the practical channel models well preserve the system performances obtained for our theoretical model, especially in high SNR regime. Note that in Fig. 6, we set $D = 4$ and 8 for the channels with $T_S = 2$ ns and $T_S = 1$ ns, respectively, to ensure that their baud rates (i.e. B/D) are the same for a fair comparison of the two. As seen from this comparison, a channel's multi-path richness (or higher resolution of perceiving multiple paths) due to the broader system bandwidth, gives rise to better user-separation in the proposed TRDMA scheme, which in essence increases the degree of freedom of the location-specific signatures.

IV. Achievable Rates

In this section, we evaluate the proposed TRDMA in terms of achievable rates. We first look at its achievable sum rate. Then, two types of achievable rates with ϵ-outage are defined and analyzed. Finally, we derive the two-user achievable rate region of the TR structure and compare it with its rake-receiver counterparts.

A. Achievable sum rate

The achievable sum rate can be used as an important metric of the efficiency of a wireless downlink scheme, which measures the total amount of information that can be effectively delivered given the total transmit power constraint P.

When the total transmit power is P, the variance of each symbol is limited to $\theta = PD/N$, according to the simple conversion shown in (11). For any instantaneous realization of the random channels that we modeled in Section II, one could obtain its corresponding instantaneous effective SINR of user i with symbol variance θ using the following equation

$$SINR(i,\theta) \triangleq \frac{P_{Sig}(i)}{P_{ISI}(i) + P_{IUI}(i) + \sigma^2}, \tag{30}$$

where each term is specified in (16), (17) and (18).

Then, under the total power constraint P, the instantaneous achievable rate of user i can be calculated as

$$\begin{aligned} R(i) &= \frac{\eta}{T_S \times B \times D} \log_2\left(1 + SINR(i, PD/N)\right) \\ &= \frac{\eta}{D} \log_2\left(1 + SINR(i, PD/N)\right) \quad (bps/Hz), \end{aligned} \tag{31}$$

where η serves as a discount factor that describe the proportion of the transmission phase in the entire duty cycle. We normalize the sum rate with bandwidth $B = 1/T_S$, presenting the information rate achieved per unit bandwidth (often referred to as *spectral efficiency*). It is also worth noting that in (31), the quantity is divided by D, because of the consequence of rate back-off.

Accordingly, the instantaneous achievable sum rate can be obtained as

$$R = \sum_{i=1}^{N} R(i) = \frac{\eta}{D} \sum_{i=1}^{N} \log_2\left(1 + SINR(i, PD/N)\right). \tag{32}$$

Averaging (32) over all realizations of the random ergodic channels, the expected value of the instantaneous achievable

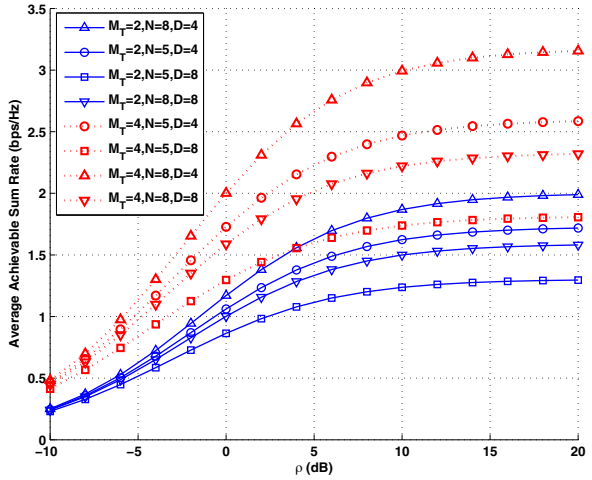

Fig. 7. The normalized achievable sum rate versus ρ.

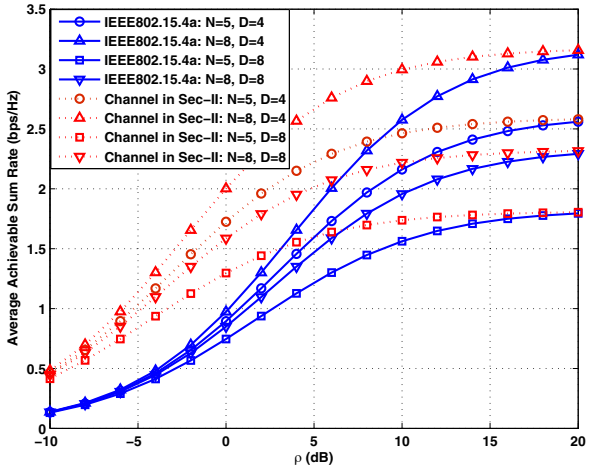

Fig. 8. The normalized achievable sum rate for IEEE 802.15.4a outdoor NLOS channel models.

sum rate is a good reference of the long-term performance and can be calculated by

$$R_{avg} = E\left[\frac{\eta}{D}\sum_{i=1}^{N}\log_2\left(1+SINR(i,PD/N)\right)\right]. \quad (33)$$

In the following part of this section, without loss of generality, we use $\eta \approx 1$, ignoring the overhead caused by the recording phase in each duty cycle, which is valid when the fading channels are not varying very fast.

The numerical evaluation of the average achievable sum rate is shown with the CIR length $L = 257$ and delay spread $\sigma_T = 128T_S$ in the system model. We plot this average achievable sum rate (setting $\eta = 1$) in Fig. 7 with different system configurations. To show how well the scheme performs in more realistic environments, we also include a comparison of the achievable-sum-rate performances for the channel model (with $L = 257$, $\sigma_T = 128T_S$, and $M_T = 4$) introduced in Section II and the IEEE802.15.4a Outdoor NLOS channel model (with $B = 1$ GHz, $T_S = 1$ ns, $M_T = 4$) in Fig. 8.

From Fig. 7, one can see that the sum rate increases monotonically with M_T, as a result of improved SINRs achieved by enhanced spatial focusing. From Fig. 8, one can see that the IEEE802.15.4a channel model with comparable channel length ($L \sim 200$ to 300 taps) well preserves the achievable sum rates of the theoretical channel model introduced in Section II, especially in high SNR regime. This demonstrates the effectiveness of TRDMA when applied to more practical channels. From both Fig. 7 and Fig. 8, one can see that a larger N gives rise to a larger achievable sum rate, and a larger D discounts the achievable sum rate. The mechanisms of how D and N affect the sum rate are summarized as follows:

- A larger N increases the concurrent data streams (or multiplexing order), while degrades the individual achievable rate of each user due to stronger interference among users. The SINR degradation is inside the logarithm function in (32), but the multiplexing order multiplies logarithm function, yielding a higher sum rate when N is larger.
- On the other hand, a larger D improves the reception quality of each symbol as a result of reduced ISI, but it lowers the symbol rate of the transmitter. For similar reasons, the improvement of SINR inside the logarithm function cannot compensate the loss of lowering symbol rate.

Thus, a choice of the pair (D, N) can reveal a fundamental engineering tradeoff between the signal quality at each user and the sum rate of this network.

B. Achievable Rate with ϵ-outage

In this part, we look at the achievable rate with ϵ-outage of the TRDMA-based multi-user network. The concept of ϵ-*outage rate*[4], [30] allows bits sent over random channels to be decoded with some probability of errors no larger than ϵ, namely the *outage probability*. Such a concept well applies to slow-varying channels, where the instantaneous achievable rate remains constant over a large number of transmissions, as is typically the case when the TR-structure is applied.

We first define two types of outage events in the TRDMA-based downlink network, and then characterize the outage probability of each type.

Definition 1. (Outage of type I (individual rate outage)) *We say* outage of type I *occurs at user i if the achievable rate of user i, as a random variable, is less than a given transmission rate R, i.e. the outage event of type I can be formulated as $\left\{\frac{1}{D}\log_2(1+SINR(i,\theta)) < R\right\}$, and the corresponding outage probability of user i for rate R is*

$$P_{out\_I}(i) = Pr\left\{\frac{1}{D}\log_2(1+SINR(i,\theta)) < R\right\}, \quad (34)$$

where $SINR(i,\theta)$ is given by (30) with the variance of each information symbol $\theta = PD/N$.

Definition 2. (Outage of type II (average rate outage)) *We say* outage of type II *occurs if the rate achieved per user (averaged over all the users) in the network, as a random variable, is less than a given transmission rate*

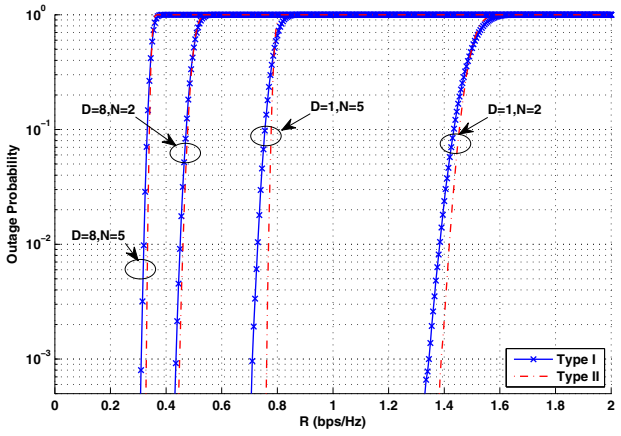

Fig. 9. The normalized achievable rate with outage.

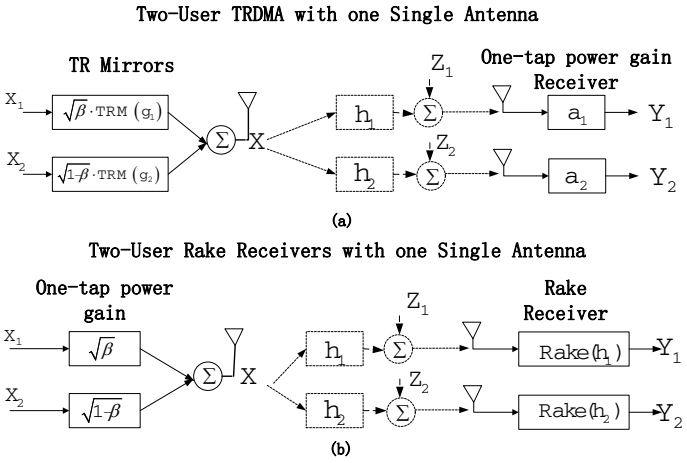

Fig. 10. Two downlink systems.

R, *i.e. the outage event of type II can be formulated as* $\left\{\frac{1}{N}\sum_{i=1}^{N}\frac{1}{D}\log_2\left(1+SINR(i,\theta)\right)<R\right\}$, *and the corresponding outage probability for rate* R *is*

$$P_{out\_II}=Pr\left\{\frac{1}{D\cdot N}\sum_{i=1}^{N}\log_2\left(1+SINR(i,\theta)\right)<R\right\}, \quad (35)$$

where $SINR(i,\theta)$ *is given by (30) with the variance of each information symbol* $\theta=PD/N$.

We present the two types of outage probabilities as functions of the transmission rate R in Fig. 9. Without loss of generality (due to symmetry), we select user 1's type-I outage probability P_{out_I} as a representative of others. In Fig. 9, simulation is made with $L=257$ and $\sigma_T=128T_S$ under the normalized SNR level $\rho=10dB$. As one can see, the slopes of curves in Fig. 9 are all very steep before the outage probabilities approach to 1. This indicates that the TR transmission technology could effectively combat the multi-path fading and makes the system behave in a more deterministic manner due to the *strong law of large numbers*. Such a property is highly desirable in a broad range of wireless communications, where link stability and reliability are prior concerns. Also, similar discounting effect on the achievable rate of rate back-off D is observed, and a larger N (number of users) would also reduce the individual achievable rate with the same outage probability due to its resulting larger IUI.

C. Achievable Rate Region Improvement over Rake receivers

In this part, we present TRDMA's improvement of achievable rate region over its counterpart, the rake receivers. Note that in the single-user case, by shifting the equalization from the receiver to the transmitter, time reversal bears some mathematical similarity to the rake receivers whose number of fingers is equal or close to the length of channel impulse response. However, as shown in [5], for some broadband communications with typically tens to hundreds of paths, the complexity of rake receiver with such a large number of fingers is not practical. We demonstrate the advantage of TR structure over rake receivers in a multi-user scenario where spatial focusing effect of TR structure plays an important role, with the derivation of the two-user achievable rate region (the case of more users can be extended by defining a region in higher dimensional space). Specifically, we look at the TRDMA scheme and rake-receiver-based schemes in terms of the amount of information delivered (mutual information between input and output) within one single transmission, measured by bits per use of the multi-path channel.

Consider a two-user downlink scenario, where the transmitter has two independent information symbols X_1 and X_2 for two different receivers, respectively. The links between the transmitter and each receiver are modeled as a discrete multi-path channel with impulse responses h_1 and h_2 as in Section II. Fig. 10 (a) shows a two-user single-antenna TRDMA scheme as introduced in this paper; and Fig. 10 (b) shows a two-user rake-receiver based downlink solution. As we will show later, the proposed TRDMA scheme outperforms the rake-receiver based schemes even when we assume that the number of fingers can be equal to the length of channel impulse response and that the delay, amplitude and phase of each path can be perfectly tracked by the rake receiver.

1) Rake Receivers: For the ideal rake receivers in Fig. 10 (b), the equalized signals can be written as

$$Y_1=||h_1||_2X+Z_1; \quad Y_2=||h_2||_2X+Z_2, \quad (36)$$

where $||h_i||_2=\sqrt{\sum_{l=0}^{L-1}|h_i(l)|^2}$ is the Euclidean norm of the channel impulse response h_i, and Z_i is additive white Gaussian noise with zero-mean and variance σ_i^2. X is the transmitted signal, which is the combination of the two information symbols X_1 and X_2.

One of the most intuitive way of combining X_1 and X_2 is to use orthogonal bases that allocate each user a fraction of the total available degrees of freedom[31]. In the two-user case, suppose that $X(t)=\sqrt{\beta}X_1c_1(t)+\sqrt{1-\beta}X_2c_2(t)$ where $c_1(t)$ and $c_2(t)$ are two orthonormal basis functions that assign a fraction $\alpha\in(0,1)$ of the total available degrees of freedom to user 1 and $(1-\alpha)$ to user 2. We consider the two-user achievable rate region with a total transmit power constraint. Specifically, let us assume that X_1 and X_2 are independent and identically distributed (i.i.d.) random variables with variance Φ, with the power allocation factor β such that the variance

of X $var(X) = \left(\sqrt{\beta}\right)^2 \Phi + \left(\sqrt{1-\beta}\right)^2 \Phi = \Phi$.

Then, for the ideal rake receivers using orthogonal bases, the maximum achievable rate pair (R_1, R_2) in *bits per channel use* is given by[30]

$$\begin{aligned} R_1 &\le \alpha \log_2 \left(1 + \frac{\beta ||h_1||_2^2 \Phi}{\alpha \sigma_1^2}\right) \\ R_2 &\le (1-\alpha) \log_2 \left(1 + \frac{(1-\beta)||h_2||_2^2 \Phi}{(1-\alpha)\sigma_2^2}\right), \end{aligned} \tag{37}$$

with all possible values $\alpha \in (0,1)$ and $\beta \in [0,1]$ defining the achievable rate region.

It has been shown that for the input-output correspondence shown in (36), the optimal frontier of the concurrently achievable rate pair is characterized by using superposition coding[32]–[35]. Without loss of generality, we assume that $\frac{\sigma_1^2}{||h_1||_2^2} \le \frac{\sigma_2^2}{||h_2||_2^2}$, i.e. User 1's channel is advantageous to User 2's. Then the achievable rate region of the superposition coding is given by[30]

$$\begin{aligned} R_1 &\le \log_2 \left(1 + \frac{\beta ||h_1||_2^2 \Phi}{\sigma_1^2}\right) \\ R_2 &\le \log_2 \left(1 + \frac{(1-\beta)||h_2||_2^2 \Phi}{\beta ||h_2||_2^2 \Phi + \sigma_2^2}\right) \end{aligned} \tag{38}$$

where $\beta \in [0,1]$ is the power allocation factor that defines the achievable rate region.

2) TRDMA Scheme and Genie-aided Outer-bound: For the TRDMA scheme with a single-tap receiver, when just one single transmission is considered, the input-and-output correspondence is reduced to

$$\begin{aligned} Y_1 &= \sqrt{\beta}||h_1||_2 X_1 + \sqrt{1-\beta}\,(h_1 * g_2)\,(L-1)\,X_2 + Z_1; \\ Y_2 &= \sqrt{1-\beta}||h_2||_2 X_2 + \sqrt{\beta}\,(h_2 * g_1)\,(L-1)\,X_1 + Z_2, \end{aligned} \tag{39}$$

where $g_i(l) = h_i^*(L-1-l)/||h_i||_2$ implemented by TRMs, and $(h_j * g_i)$ denotes the convolution of h_j and g_i.

Then, the resulting mutual information is obtained as follows

$$\begin{aligned} R_1 &\le \log_2 \left(1 + \frac{||h_1||_2^2 \beta \Phi}{|(h_1 * g_2)(L-1)|^2 (1-\beta)\Phi + \sigma_1^2}\right) \\ R_2 &\le \log_2 \left(1 + \frac{||h_2||_2^2 (1-\beta)\Phi}{|(h_2 * g_1)(L-1)|^2 \beta \Phi + \sigma_2^2}\right) \end{aligned} \tag{40}$$

where $\beta \in [0,1]$ is the power allocation factor that defines the achievable rate region.

Lastly, we derive a genie-aided outer-bound for the two-user capacity region, in which case all the interference is assumed to be known and thus can be completely removed. Such a genie-aided outer-bound can be obtained with $\beta \in [0,1]$ as follows

$$\begin{aligned} R_1 &\le \log_2 \left(1 + \frac{||h_1||_2^2 \beta \Phi}{\sigma_1^2}\right) \\ R_2 &\le \log_2 \left(1 + \frac{||h_2||_2^2 (1-\beta)\Phi}{\sigma_2^2}\right) \end{aligned} \tag{41}$$

3) Numerical Comparison: We present a numerical comparison of the capacity regions obtained in (37) (38) (40) and (41). In particular, we set $\frac{\Phi\ E\left[||h_1||_2^2\right]}{\sigma_1^2} = 10dB$ for User 1 and $\frac{\Phi\ E\left[||h_2||_2^2\right]}{\sigma_2^2} = 5dB$ for User 2. In Fig. 11, results are obtained by averaging over 1000 trials of multi-path Rayleigh fading channels. Each time, channel impulse responses h_1 and h_2 are randomly generated with parameters $L = 257$ and $\sigma_T = 128 T_S$ according to the channel model in Section II.

First, in Fig. 11, all the schemes achieve the same performances in the degraded single-user case, which corresponds to the two overlapping intersection points on the axes. This is due to the mathematical similarity between TR and Rake receivers in the single-user case and the commutative property of linear time-invariant (LTI) system. On the other hand, in most cases when both users are active, the proposed TRDMA scheme outperforms all the rake-receiver based schemes as shown in Fig. 11. Moreover, the frontier achieved by TRDMA is close to the Genie-aided outer-bound. All these demonstrate TRDMA's unique advantage of spatial focusing brought by the pre-processing of embedding location-specific signatures before sending signals into the air. The high-resolution spatial focusing, as the key mechanism of the TRDMA, alleviates interference between users and provides a novel wireless medium access solution for multi-user communications.

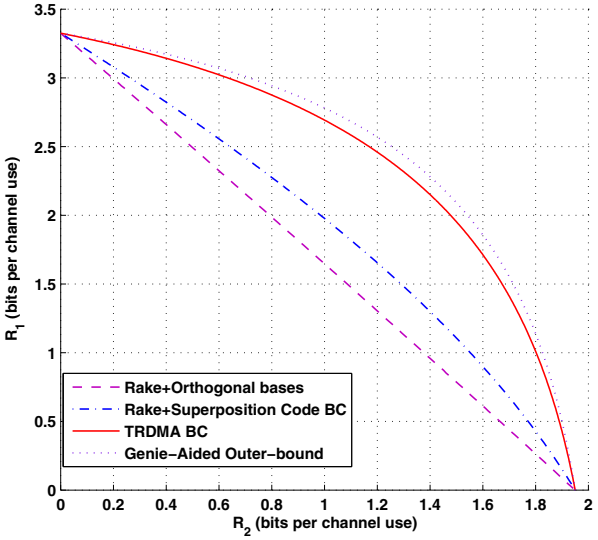

Fig. 11. Achievable rate region for two-user case.

V. Channel Correlation Effect

In the preceding sections, we assume a model of independent channels, because for rich-scattering multi-path profiles associated with reasonably far-apart (typically, several wavelengths) locations, they are often highly uncorrelated[19]. However, channels may become correlated when the environment is less scattering and users are very close to each other. To gain a more comprehensive understanding of TRDMA, it is also interesting and important to develop a quantitative assessment of its performance degradation due to spatial correlation between users.

A. Spatial Channel Correlation

Although there are many ways to model correlated channel responses, we herein choose to obtain correlated channel responses $\widehat{X}$ and $\widehat{Y}$ by performing element-wise linear combinations of independent channels X and Y as follows[36]–[38]

$$\begin{bmatrix} \widehat{X}(i) \\ \widehat{Y}(i) \end{bmatrix} = \begin{bmatrix} \sqrt{\xi} & \sqrt{1-\xi} \\ \sqrt{1-\xi} & \sqrt{\xi} \end{bmatrix} \begin{bmatrix} X(i) \\ Y(i) \end{bmatrix}, \tag{42}$$

where the coefficient $\xi \in [0,1]$.

Before we proceed, we give a definition to *spatial correlation* of two multi-path channel responses.

$$E\left[\widehat{P}_{IUI}(i)\right] = \left[\xi^2+(1-\xi)^2\right]E\left[P_{IUI}(i)\right] + 2\xi(1-\xi)\left(E\left[P_{Sig}(i)\right]+E\left[P_{ISI}(i)\right]+\theta E\left[\sum_{l=0}^{L-1}|h_i[l]|^2\right]\right)$$
$$= E\left[P_{IUI}(i)\right] + \frac{S^2_{\widehat{h}_1\widehat{h}_2}}{2}\left(E\left[P_{Sig}(i)\right]+E\left[P_{ISI}(i)\right]-E\left[P_{IUI}(i)\right]+\theta E\left[\sum_{l=0}^{L-1}|h_i[l]|^2\right]\right), \quad (46)$$

Definition 3. *For two multi-path channel responses $\widehat{X}$ and $\widehat{Y}$, the spatial correlation of $\widehat{X}$ and $\widehat{Y}$ is defined as*

$$S_{\widehat{X}\widehat{Y}} = \frac{\sum_{i=0}^{L-1}\left|E\left[\widehat{X}(i)\widehat{Y}(i)^*\right]\right|}{\sqrt{\sum_{i=0}^{L-1}E\left[|\widehat{X}(i)|^2\right]\cdot\sum_{j=0}^{L-1}E\left[|\widehat{Y}(j)|^2\right]}}. \quad (43)$$

Note that this definition assumes zero-mean channel responses without loss of generality, and $S_{\widehat{X}\widehat{Y}}$ takes values between 0 and 1. Particularly, when $\widehat{X}$ and $\widehat{Y}$ are identical or additive inverse to each other, $S_{\widehat{X}\widehat{Y}}=1$; when $\widehat{X}$ and $\widehat{Y}$ are uncorrelated, $S_{\widehat{X}\widehat{Y}}=0$.

B. Channel correlation among users

For simplicity, we look at a two-user SISO case with correlated channel responses. We observe the impact of users' spatial correlation to the system performances.

Let us consider two correlated CIRs $\widehat{h}_1$ and $\widehat{h}_2$ obtained from the linear combination of two independent CIRs h_1 and h_2, as shown in (42), where $h_i[k]$'s are assumed as in Section II to be independent circular symmetric complex Gaussian random variables with zero mean and variance $E[|h_i[k]|^2] = e^{-\frac{kT_S}{\sigma_T}}$, for $0 \le k \le L-1$.

Then, the spatial correlation defined in (43) for $\widehat{h}_1$ and $\widehat{h}_2$ can be calculated by the simple form

$$S_{\widehat{h}_1\widehat{h}_2} = 2\sqrt{\xi(1-\xi)}. \quad (44)$$

Since the spatial correlation only affects the inter-user interference power, here we focus on the change of the average power of IUI as a result of channel correlations. Similar to (18), the expected value of the new IUI power $\widehat{P}_{IUI}(i)$ at User i in such a two-user SISO case (i.e. $N=2$ and $M_T=1$) with the correlated CIRs $\widehat{h}_1$ and $\widehat{h}_2$ can be written as

$$E\left[\widehat{P}_{IUI}(i)\right] = \theta E\left[\sum_{l=0}^{\frac{2L-2}{D}}\left|\left(\widehat{h}_i * \widehat{g}_j\right)[Dl]\right|^2\right], \quad (45)$$

where $j \ne i$ $(i,j \in \{1,2\})$, and the TRM

$$\widehat{g}_j[k] = \widehat{h}_j^*[L-1-k] \Big/ \sqrt{E\left[\sum_{l=0}^{L-1}\left|\widehat{h}_j[l]\right|^2\right]}$$

corresponds to User j with the CIR $\widehat{h}_j$.

A direct calculation of (45) can be tedious. However, by substituting uncorrelated h_1 and h_2 into (45) according to the linear transform (42), we can utilize the existing results in Section III and represent the expected value of $\widehat{P}_{IUI}(i)$ in terms of $E\left[P_{Sig}(i)\right]$, $E\left[P_{ISI}(i)\right]$, and $E\left[P_{IUI}(i)\right]$ in (20-22) calculated with respect to uncorrelated h_1 and h_2, as presented in (46).

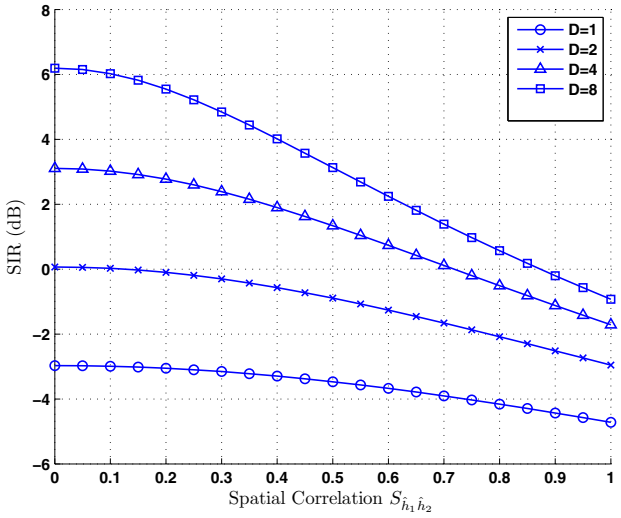

Fig. 12. SIR vs spatial correlation with $N=2$ and $M_T=1$.

Note that in (46), the second term $\left(E\left[P_{Sig}(i)\right]+E\left[P_{ISI}(i)\right]-E\left[P_{IUI}(i)\right]+\theta E\left[\sum_{l=0}^{L-1}|h_i[l]|^2\right]\right)$ is always positive, which is a penalty to the system performance due to the two users' spatial correlation. When $S_{\widehat{h}_1\widehat{h}_2}=0$ (i.e. $\xi=0$ or $\xi=1$), $\widehat{h}_1$ and $\widehat{h}_2$ are uncorrelated, and thus $E\left[\widehat{P}_{IUI}(i)\right] = E\left[P_{IUI}(i)\right]$. In the extreme case when $S_{\widehat{h}_1\widehat{h}_2}=1$ (i.e. $\xi=0.5$) that maximizes (46), $\widehat{h}_1$ and $\widehat{h}_2$ are identical, the IUI achieves its upper-bound

$$E\left[\widehat{P}_{IUI}(i)\right] = \frac{E\left[P_{Sig}(i)+P_{ISI}(i)+P_{IUI}(i)\right]+\theta E\left[\sum_{l=0}^{L-1}|h_i[l]|^2\right]}{2}. \quad (47)$$

Since $E\left[P_{Sig}(i)+P_{ISI}(i)\right] = E\left[P_{IUI}(i)\right]+\theta E\left[\sum_{l=0}^{L-1}|h_i[l]|^2\right]$ at $D=1$, (47) can be written as $E\left[\widehat{P}_{IUI}(i)\right] = E\left[P_{Sig}(i)\right]+E\left[P_{ISI}(i)\right]$, when there is no rate back-off.

The impact of the increased interference would be most prominent in the high SNR regime, where the interference power dominates the noise power. So we evaluate its impact to the system performance in terms of signal-to-interference ratio (SIR), as a close approximation of the effective SINR in high SNR regime. Fig. 12 shows the influence of the spatial correlation to the SIR with correlated CIRs $\widehat{h}_1$ and $\widehat{h}_2$ of length $L=257$ and delay spread $\sigma_T = 128T_S$. As one can see in

Fig. 12, the SIR degradation speed varies with different ranges of $S_{\widehat{h}_1\widehat{h}_2}$. In the lower range of $S_{\widehat{h}_1\widehat{h}_2}$ (e.g. from 0 to 0.2) the SIR degrades very slowly. Also, the larger rate back-off D tends to result in a faster performance loss due to spatial correlation as shown in Fig. 12. However, even for $S_{\widehat{h}_1\widehat{h}_2}$ up to 0.5 which is rare in real-life RF communications over scattering environments, the degraded SIR is preserved within $3dB$ away from the performances of uncorrelated channels. This demonstrates the robustness of the proposed TRDMA scheme and provides a more comprehensive understanding of its system performances.

VI. Conclusion

In this paper, we proposed a TRDMA scheme for the multi-user downlink network over multi-path channels. Both single-antenna and multi-antenna schemes were developed to utilize the location-specific signatures that naturally exist in the multi-path environment. We defined and evaluated both analytically and numerically a variety of performance metrics of including the effective SINR, the achievable sum rate, and achievable rates with outage. We then demonstrated the TRDMA's improvement of achievable rate region over the rake receivers and investigated the impact of spatial correlations between users to the system performances. Based on the nice properties shown in the analysis and simulation results of this paper, the proposed TRDMA can be a promising technique in the future energy-efficient low-complexity broadband wireless communications.

References

[1] J. G. Proakis, *Digital Communications*, 4th edition. McGraw-Hill, 2001.

[2] G. L. Stuber, *Principles of Mobile Communications*, 2nd edition. Kluwer, 2001.

[3] A. J. Goldsmith, *Wireless Communication*. Cambridge University Press, 2005.

[4] D. Tse and P. Viswanath, *Fundamental of Wireless Communication*. Cambridge University Press, 2005.

[5] B. Wang, Y. Wu, F. Han, Y. H. Yang, and K. J. R. Liu, "Green wireless communications: a time-reversal paradigm," *IEEE J. Sel. Areas Commun.*, vol. 29, no. 8, pp. 1698–1710, Sep. 2011.

[6] M. Fink, C. Prada, F. Wu, and D. Cassereau, "Self focusing in inhomogeneous media with time reversal acoustic mirrors," in *Proc. 1989 IEEE Ultrasonics Symp.*, vol. 1, pp. 681–686.

[7] C. Prada, F. Wu, and M. Fink, "The iterative time reversal mirror: a solution to self-focusing in the pulse echo mode," *J. Acoustic Society America*, vol. 90, pp. 1119–1129, 1991.

[8] M. Fink, "Time reversal of ultrasonic fields—part I: basic principles," *IEEE Trans. Ultrasonic, Ferroelectron., Frequency Control*, vol. 39, pp. 555–566, Sep. 1992.

[9] C. Dorme and M. Fink, "Focusing in transmit-receive mode through inhomogeneous media: the time reversal matched filter approach," *J. Acoustic Society America*, vol. 98, no. 2, part 1, pp. 1155–1162, Aug. 1995.

[10] A. Derode, P. Roux, and M. Fink, "Robust acoustic time reversal with high-order multiple scattering," *Phys. Rev. Lett.*, vol. 75, pp. 4206–4209, 1995.

[11] W. A. Kuperman, W. S. Hodgkiss, and H. C. Song, "Phase conjugation in the ocean: experimental demonstration of an acoustic time-reversal mirror," *J. Acoustic Society America*, vol. 103, no. 1, pp. 25–40, Jan. 1998.

[12] H. C. Song, W. A. Kuperman, W. S. Hodgkiss, T. Akal, and C. Ferla, "Iterative time reversal in the ocean," *J. Acoustic Society America*, vol. 105, no. 6, pp. 3176–3184, June 1999.

[13] D. Rouseff, D. R. Jackson, W. L. Fox, C. D. Jones, J. A. Ritcey, and D. R. Dowling, "Underwater acoustic communication by passive-phase conjugation: theory and experimental results," *IEEE J. Oceanic Eng.*, vol. 26, pp. 821–831, 2001.

[14] A. Derode, A. Tourin, J. de Rosny, M. Tanter, S. Yon, and M. Fink "Taking advantage of multiple scattering to communicate with time-reversal antennas," *Phys. Rev. Lett.*, vol. 90, pp. 014301-1–014301-4, 2003.

[15] D. Rouseff, D. R. Jackson, W. L. J. Fox, C. D. Jones, J. A. Ritcey, and D.R. Dowling, "Underwater acoustic communication by passive-phase conjugation: theory and experimental results," *IEEE J. Oceanic Eng.*, vol. 26, pp. 821–831, 2001.

[16] G. F. Edelmann, T. Akal, W. S. Hodgkiss, S. Kim, W. A. Kuperman, and H. C. Song, "An initial demonstration of underwater acoustic communication using time reversal," *IEEE J. Oceanic Eng.*, vol. 27, pp.602–609, 2002.

[17] S. M. Emami, J. Hansen, A. D. Kim, G. Papanicolaou, and A. J. Paulraj, "Predicted time reversal performance in wireless communications," *IEEE Commun. Lett.*, 2004.

[18] M. Emami, M. Vu, J. Hansen, A. J. Paulraj, and G. Papanicolaou, "Matched filtering with rate back-off for low complexity communications in very large delay spread channels," in *Proc. Asilomar Conf. Signals, Syst. Comput.*, vol. 1, pp. 218–222.

[19] K. F. Sander and G. A. L. Reed, *Transmission and Propagation of Electromagnetic Waves*, 2nd edition. Cambridge University Press, 1986.

[20] H. T. Nguyen, I. Z. Kovacs, and P. C. F. Eggers, "A time reversal transmission approach for multiuser UWB communications," *IEEE Trans. Antennas Propag.*, vol. 54, no. 11, pp. 3216–3224, Nov. 2006.

[21] I. H. Naqvi, A. Khaleghi, and G. E. Zein, "Performance enhancement of multiuser time reversal UWB communication system," *2007 IEEE International Symp. Wireless Commun. Syst.* [http://arXiv:0810.1506v1[cs.NI]].

[22] H. T. Nguyen, "Partial one bit time reversal for UWB impulse radio multi-user communications," in *Proc. 2008 International Conf. Commun. Electron.*, pp. 246–251.

[23] H. Nguyen, Z. Zhao, F. Zheng, and T. Kaiser, "Pre-equalizer design for spatial multiplexing SIMO UWB systems," *IEEE Trans. Veh. Technol.*, vol. 59, no. 8, pp. 3798–3805, Oct. 2010.

[24] T. K. Nguyen, H. Nguyen, F. Zheng, and T. Kaiser, "Spatial correlation in SM-MIMO-UWB systems using a pre-equalizer and pre-rake filter," *2010 IEEE International Conf. Ultra-Wideband*.

[25] T. K. Nguyen, H. Nguyen, F. Zheng, and T. Kaiser, "Spatial correlation in the broadcast MU-MIMO UWB system using a pre-equalizer and time reversal pre-filter," *2010 International Conf. Signal Process. Commun. Syst.*

[26] A. Derode, A. Tourin, and M. Fink, "Ultrasonic pulse compression with one-bit time reversal through multiple scattering," *J. Applied Physics*, vol. 85, no. 9, May 1999.

[27] H. V. Poor and G. W Wornell, *Wireless Communications: Signal Processing Perspectives*, 1st edition. Prentice Hall, 1998.

[28] P. H. Moose, "A technique for orthogonal frequency division multiplexing frequency offset correction," *IEEE Trans. Commun.*, vol. 42, no. 10, pp. 2908–2914, Oct. 1994.

[29] J. Lee, H.-ling Lou, D. Toumpakaris, and J. M. Cioffi, "SNR analysis of OFDM systems in the presence of carrier frequency offset for fading channels," *IEEE Trans. Wireless Commun.*, vol. 5, no. 12, pp. 3360–3364, Dec. 2006

[30] T. M. Cover and J. A. Thomas, *Elements of Information Theory*. John Wiley & Sons, 2006.

[31] J. L. Massey, "Towards an information theory of spread-spectrum systems," in *Code Division Multiple Access Communications*, S. G. Glisic and P. A. Leppanen, editors, pp. 29–46. Kluwer Academic Publishers, 1995.

[32] T.M. Cover, "Broadcast channels," *IEEE Trans. Inf. Theory*, vol. IT-18, no. 1 pp. 2–14, Jan. 1972.

[33] P. P. Bergmans, "Random coding theorem for broadcast channels with degraded components," *IEEE Trans. Inf. Theory*, vol. IT-19, no. 1 pp. 197–207, Mar. 1973.

[34] P. P. Bergmans, "A simple converse for broadcast channels with additive white Gaussian noise," *IEEE Trans. Inf. Theory*, vol. IT-20, no. 2 pp. 279–280, Mar. 1974.

[35] P. P. Bergmans and T. M. Cover, "Cooperative broadcasting," *IEEE Trans. Inf. Theory*, vol. IT-20, no. 3 pp. 317–324, Mar. 1974.

[36] A. Papoulis and U. Pillai, *Probability, Random Variables and Stochastic Processes*, 4th edition. McGraw-Hill, 2002.

[37] R. B. Ertel and J. H. Reed, "Generation of two equal power correlated Rayleigh fading envelopes," *IEEE Commun. Lett.*, vol. 2, no. 10. Oct. 1998.

[38] B. Natarajan, C. R. Nassar, and V. Chandrasekhar, "Generation of correlated Rayleigh fading envelopes for spread spectrum applications," *IEEE Commun. Lett.*, vol. 4, no. 1. Jan. 2000.

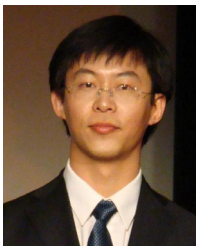

Feng Han (S'08) received the B.S. and M.S. degrees in Electronic Engineering from Tsinghua University, Beijing, China, in 2007 and 2009, respectively. He is currently pursuing the Ph. D. degree in Electrical Engineering, at the University of Maryland, College Park. His current research interests include wireless communications and networking, smart grid, game theory, and information theory.

He is a recipient of the first prize in the 19th Chinese Mathematical Olympiad, the Best Thesis Award of Tsinghua University, the honor of Excellent Graduate of Tsinghua University, the A. James Clark School of Engineering Distinguished Graduate Fellowship in 2009 and the Future Faculty Fellowship in 2012, both from the University of Maryland, College Park. He received a Best Paper Award for his work on MIMO system at IEEE WCNC'08, Las Vegas, NV, in 2008.

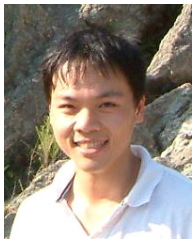

Yu-Han Yang (S'06) received his B.S. in electrical engineering in 2004, and two M.S. degrees in computer science and communication engineering in 2007, from National Taiwan University, Taipei, Taiwan. He is currently pursuing the Ph.D. degree at the University of Maryland, College Park. His research interests include wireless communication and signal processing. He received Class A Scholarship from National Taiwan University in Fall 2005 and Spring 2006. He is a recipient of Study Abroad Scholarship from Taiwan (R.O.C.) Government in 2009 and 2010.

Beibei Wang (S'07-M'11) received the B.S. degree in electrical engineering (with the highest honor) from the University of Science and Technology of China, Hefei, in 2004, and the Ph.D. degree in electrical engineering from the University of Maryland, College Park in 2009. From 2009 to 2010, she was a research associate at the University of Maryland. Currently, she is a senior engineer with Corporate Research and Development, Qualcomm Incorporated, San Diego, CA.

Her research interests include wireless communications and networking, including cognitive radios, dynamic spectrum allocation and management, network security, and heterogeneous networks. Dr. Wang was the recipient of the Graduate School Fellowship, the Future Faculty Fellowship, and the Dean's Doctoral Research Award from the University of Maryland, College Park. She is a coauthor of *Cognitive Radio Networking and Security: A Game-Theoretic View*, Cambridge University Press, 2010.

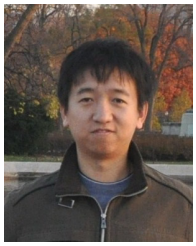

Yongle Wu (S'08-M'12) received the Ph.D. degree in Electrical and Computer Engineering from University of Maryland, College Park in 2010. He received the B.S. (with highest honor) and M.S. degrees in Electronic Engineering from Tsinghua University, Beijing, China, in 2003 and 2006, respectively.

Dr. Wu is currently a senior engineer with Qualcomm Incorporated, San Diego, CA. His research interests are in the areas of wireless communications and networks, including cognitive radio techniques, dynamic spectrum access, network security, and MIMO-OFDM communication systems.

Dr. Wu received the Graduate School Fellowship from the University of Maryland in 2006, the Future Faculty Fellowship in 2009 and the Litton Industries Fellowship in 2010, both from A. James Clark School of Engineering, University of Maryland, and the Distinguished Dissertation Fellowship from Department of Electrical and Computer Engineering, University of Maryland in 2011.

K. J. Ray Liu (F'03) is named a Distinguished Scholar-Teacher of University of Maryland, College Park, in 2007, where he is Christine Kim Eminent Professor of Information Technology. He serves as Associate Chair and Director of Graduate Studies and Research of Electrical and Computer Engineering Department and leads the Maryland Signals and Information Group conducting research encompassing broad areas of signal processing and communications with recent focus on cooperative communications, cognitive networking, social learning and networks, and information forensics and security.

Dr. Liu is the recipient of numerous honors and awards including IEEE Signal Processing Society Technical Achievement Award and Distinguished Lecturer. He also received various teaching and research recognitions from University of Maryland including university-level Invention of the Year Award; and Poole and Kent Senior Faculty Teaching Award and Outstanding Faculty Research Award, both from A. James Clark School of Engineering. An ISI Highly Cited Author in Computer Science, Dr. Liu is a Fellow of IEEE and AAAS.

Dr. Liu is President of IEEE Signal Processing Society where he has served as Vice President - Publications and Board of Governor. He was the Editor-in-Chief of *IEEE Signal Processing Magazine* and the founding Editor-in-Chief of *EURASIP Journal on Advances in Signal Processing*.